SUPPORTING INFORMATION: A Novel Electrical Depercolation Model for Stretchable Nanocomposite Strain Sensors

Oliver Tomes[a], Aaron Soul[a], Han Zhang[a], Emiliano Bilotti[b], Dimitrios G. Papageorgiou[a*]

[a] *School of Engineering and Materials Science, Queen Mary University of London, London, E1 4NS, UK*

[b] *Department of Aeronautics, Imperial College London, South Kensington Campus, SW7 2AZ London, UK*

1 Materials Characterisation

1.1 Filler Characterisation

In Fig. S1a and Fig. S1b, SEM micrographs of rGO platelets are shown displaying a high number of folds and wrinkles. Raman spectroscopy of the rGO filler (Fig. S1c) gave peak ratios of I_D/I_G = 1.56 which indicates a high defect density within graphene layers resulting in part from oxygen functional groups (primarily carboxyl, hydroxyl and epoxy) which remain after reduction of the graphene oxide [1]. Using XPS (Fig. S1d-f), the ratio of carbon to oxygen was measured to be 17.5, indicating high level of reduction for the rGO filler (C:O ratio typically ~2 for graphene oxide [2]).

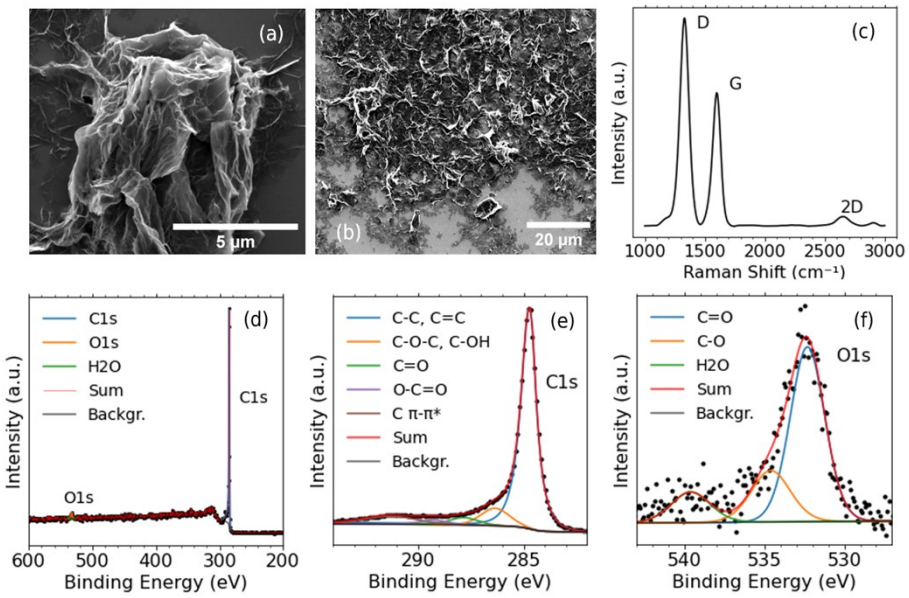

Fig. S1. Characterisation of rGO filler. (a) & (b) SEM images of rGO filler. (c) Raman showing D, G, and 2D peaks, respectively. (d) XPS survey spectrum displaying C1s and O1s peak. (e) Deconvoluted XPS C1s spectrum. (f) Deconvoluted XPS O1s spectrum.

1.2 Differential Scanning Calorimetry (DSC)

To verify the degree of cure of nanocomposite samples, DSC measurements were performed across all filler loadings and compared with that of silicone resins soon after combining to cure. All samples were tested using two consecutive ramps from 40°C to 200°C at a rate of 10°C/min. Fig. S2 depicts the resulting DSC curves. The exothermic peak detected at 140.7°C is associated with the curing reaction of the silicone rubber. No similar exothermic peaks were observed for any of the cured samples (pure SR and 0.42 vol.%, 0.52 vol.%, 0.62 vol.%, 0.70 vol.%, 0.79 vol.% SR/rGO), suggesting that the degree of cure was 100% after the specified curing regime.

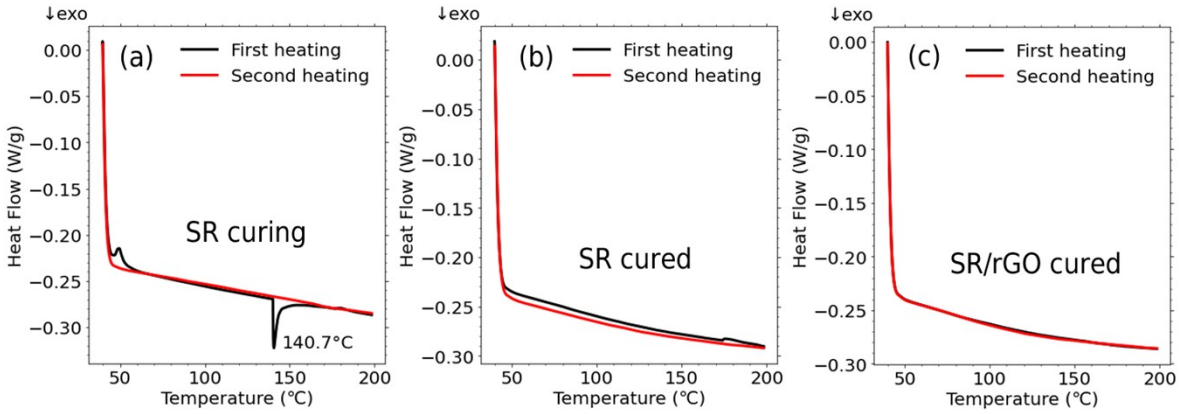

Fig. S2. DSC measurements to measure degree of cure. (a) SR during curing displaying an exothermic peak at 140.7°C due to curing reaction. (b) SR after curing. (c) Highest volume fraction of SR/rGO (0.79 vol.%) after curing.

2 Strain Sensing

2.1 Experimental Setup for Strain Sensing

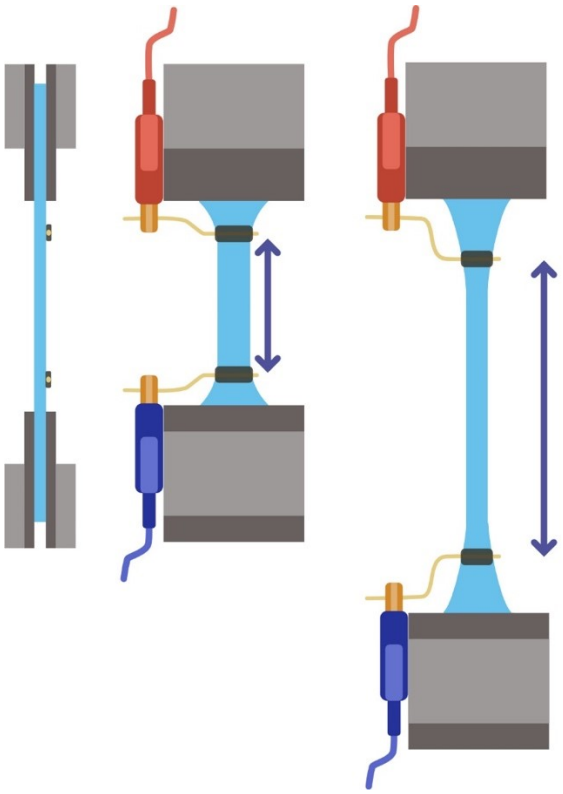

Fig. S3. Schematic depicting sample preparation for tensile strain sensing testing of ultrasoft nanocomposites. Electrodes are positioned within the gauge length in order to avoid the effect of distortion of the filler network caused by the grips. Thin copper wires, connected to multimeter, are embedded in carbon grease on the sample in order to minimise potential mechanical stresses or deformations caused by the electrodes during the measurement.

2.2 Linear Model Reduced Plot

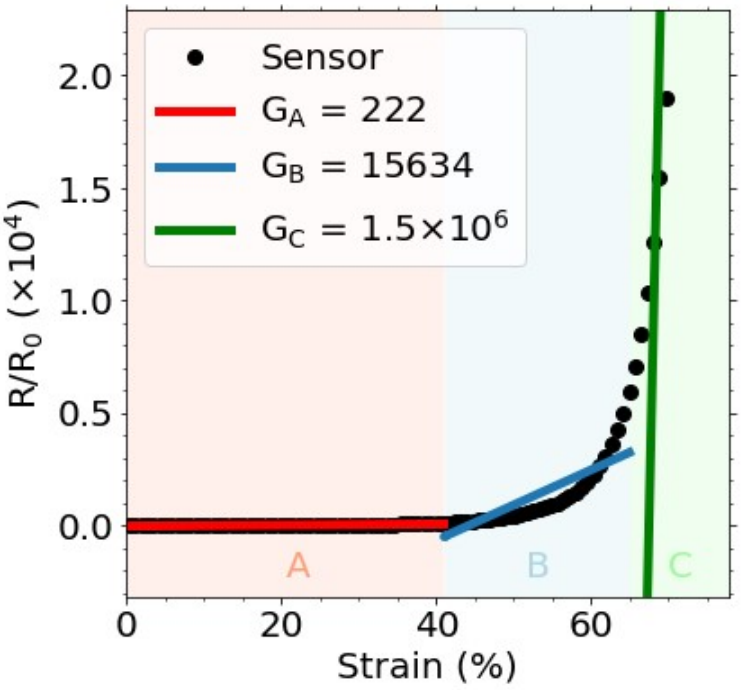

Fig. S4. Linear calibration of SR/rGO strain sensor (0.70vol.%) over initial 90% of working strain range (max $R/R_0 = 2.87\times10^5$ at 78% strain).

2.3 Comparison Of Models

Fig. S5-S9 show a comparison of calibration using three models (linear, exponential, depercolation) for each separate loading, with the top line being represented on a linear scale and bottom line shown using a logarithmic scale.

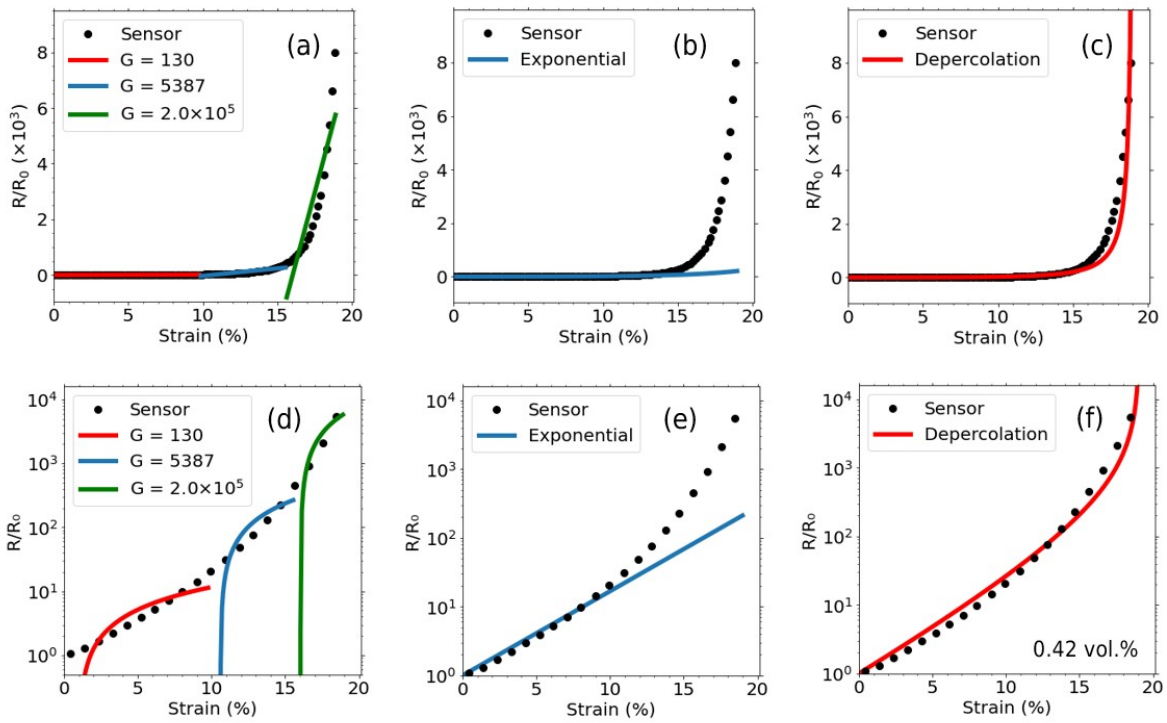

Fig. S5. Calibration of SR/rGO strain sensor with filler content of 0.42vol.%. The resistance through the sensor is measured over increasing strain until a maximum 19% strain past which the strain sensor is electrically insulating. (a) Linear stepwise calibration across full range of tensile strain. The red line represents fitting from 0% - 10% strain where the gauge factor, G, is found to be 130. The blue line represents fitting from 10% - 16% strain where the gauge factor is found to be 5.39×10^3. The green line represents fitting from 16% - 19% strain where the gauge factor is found to be 2.0×10^5. (b) Exponential calibration up to 9% strain. Past this threshold, the resistance rises faster than the exponential model is able to predict with increasing strain. (c) Calibration across full range of tensile strain using depercolation model. (d), (e) & (f) are the same as (a), (b) & (c) respectively but represented on a logarithmic scale.

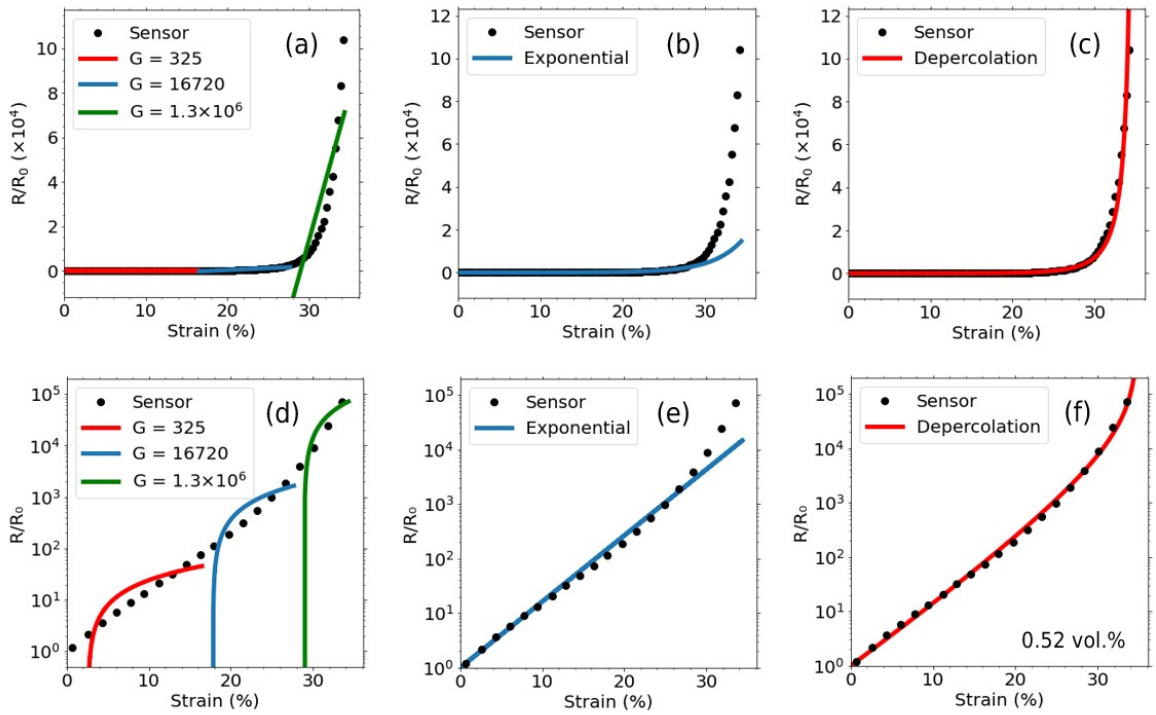

Fig. S6. Calibration of SR/rGO strain sensor with filler content of 0.52vol.%. The resistance through the sensor is measured over increasing strain until a maximum 34% strain past which the strain sensor is electrically insulating. (a) Linear stepwise calibration across full range of tensile strain. The red line represents fitting from 0% - 17% strain where the gauge factor, G, is found to be 325. The blue line represents fitting from 17% - 28% strain where the gauge factor is found to be 1.67×10^4. The green line represents fitting from 28% - 34% strain where the gauge factor is found to be 1.32×10^6. (b) Exponential calibration up to 27% strain. Past this threshold, the resistance rises faster than the exponential model is able to predict with increasing strain. (c) Calibration across full range of tensile strain using depercolation model. (d), (e) & (f) are the same as (a), (b) & (c) respectively but represented on a logarithmic scale.

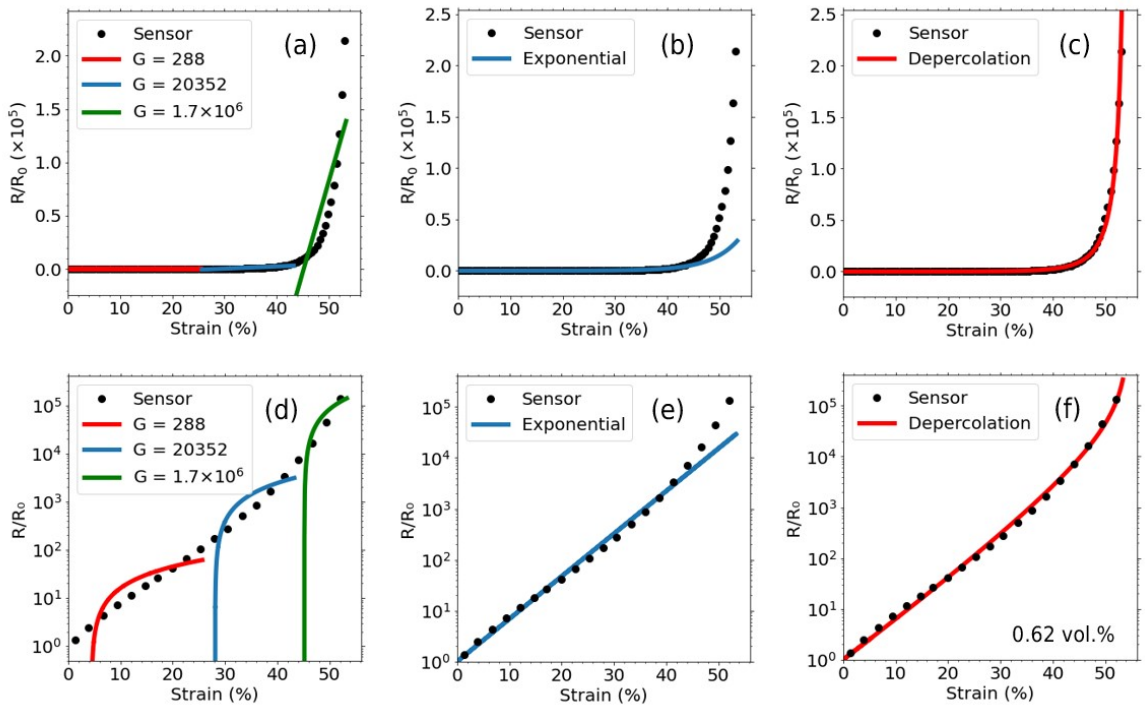

Fig. S7. Calibration of SR/rGO strain sensor with filler content of 0.62vol.%. The resistance through the sensor is measured over increasing strain until a maximum 53% strain past which the strain sensor is electrically insulating. (a) Linear stepwise calibration across full range of tensile strain. The red line represents fitting from 0% - 26% strain where the gauge factor, G, is found to be 288. The blue line represents fitting from 26% - 43% strain where the gauge factor is found to be 2.04×10^4. The green line represents fitting from 43% - 53% strain where the gauge factor is found to be 1.71×10^6. (b) Exponential calibration up to 42% strain. Past this threshold, the resistance rises faster than the exponential model is able to predict with increasing strain. (c) Calibration across full range of tensile strain using depercolation model. (d), (e) & (f) are the same as (a), (b) & (c) respectively but represented on a logarithmic scale.

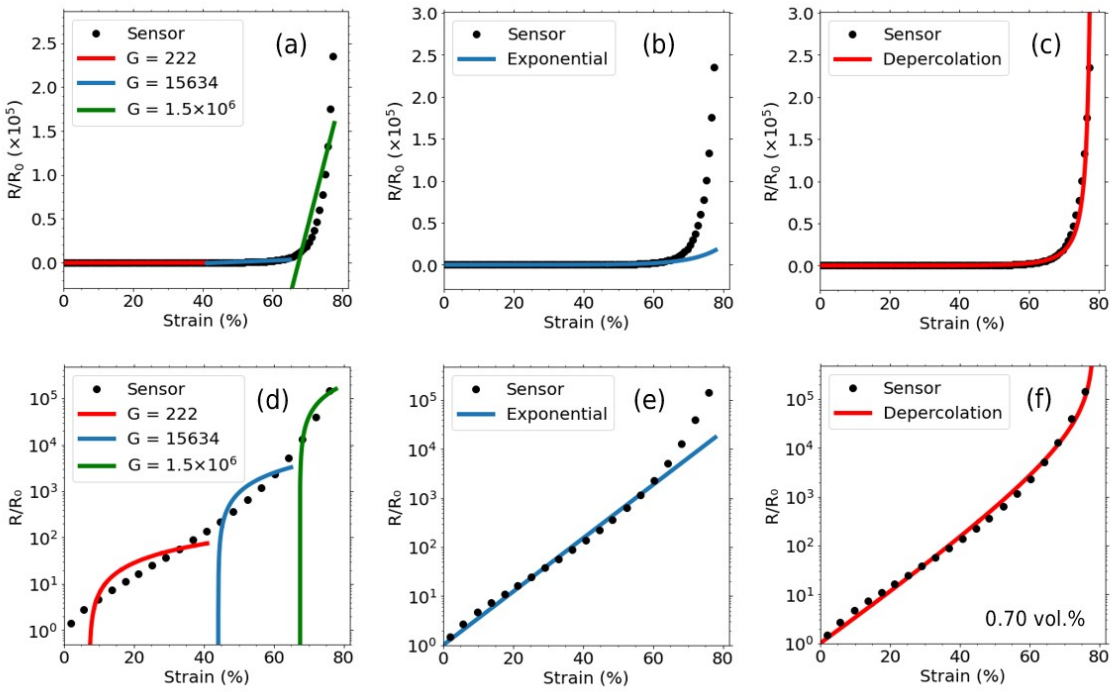

Fig. S8. Calibration of SR/rGO strain sensor with filler content of 0.70vol.%. The resistance through the sensor is measured over increasing strain until a maximum 78% strain past which the strain sensor is electrically insulating. (a) Linear stepwise calibration across full range of tensile strain. The red line represents fitting from 0% - 41% strain where the gauge factor, G, is found to be 222. The blue line represents fitting from 41% - 65% strain where the gauge factor is found to be 1.56×10^4. The green line represents fitting from 65% - 78% strain where the gauge factor is found to be 1.55×10^6. (b) Exponential calibration up to 60% strain. Past this threshold, the resistance rises faster than the exponential model is able to predict with increasing strain. (c) Calibration across full range of tensile strain using depercolation model. (d), (e) & (f) are the same as (a), (b) & (c) respectively but represented on a logarithmic scale.

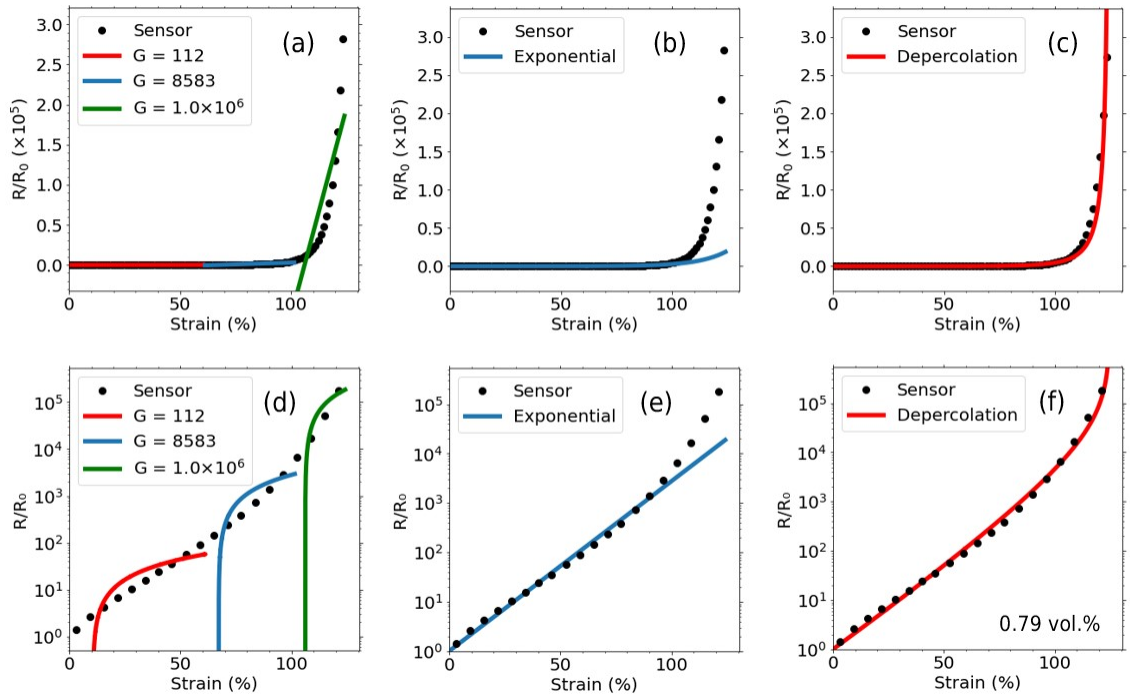

Fig. S9. Calibration of SR/rGO strain sensor with filler content of 0.79vol.%. The resistance through the sensor is measured over increasing strain until a maximum 124% strain past which the strain sensor is electrically insulating. (a) Linear stepwise calibration across full range of tensile strain. The red line represents fitting from 0% -61% strain where the gauge factor, G, is found to be 112. The blue line represents fitting from 61% - 101% strain where the gauge factor is found to be 8.58×10^3. The green line represents fitting from 101% - 124% strain where the gauge factor is found to be 1.04×10^4. (b) Exponential calibration up to 92% strain. Past this threshold, the resistance rises faster than the exponential model is able to predict with increasing strain. (c) Calibration across full range of tensile strain using depercolation model. (d), (e) & (f) are the same as (a), (b) & (c) respectively but represented on a logarithmic scale.

2.4 Electrical Depercolation Model

Fig. S10 illustrates the quality of fit of the depercolation model for all filler loadings tested in this study (0.42 vol.% - 0.79 vol.%).

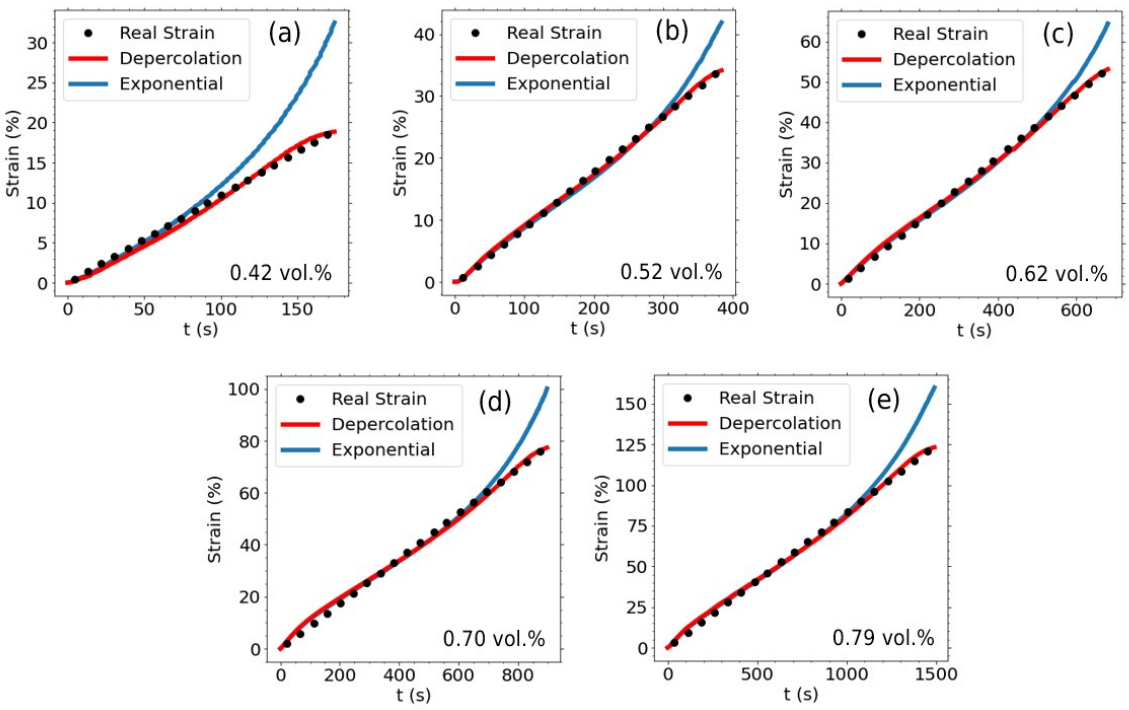

Fig. S10. Accuracy of calibration using depercolation model vs exponential model. The black dots represent the strain applied to the SR/rGO strain sensors with respective filler contents of (a) 0.42vol.% (b) 0.52vol.% (c) 0.62vol.% (d) 0.70vol.% (e) 0.79vol.%. The red line shows the strain calculated using the sensors' change in resistance calibrated using the depercolation model and the blue line gives the same calibrated using the exponential model.

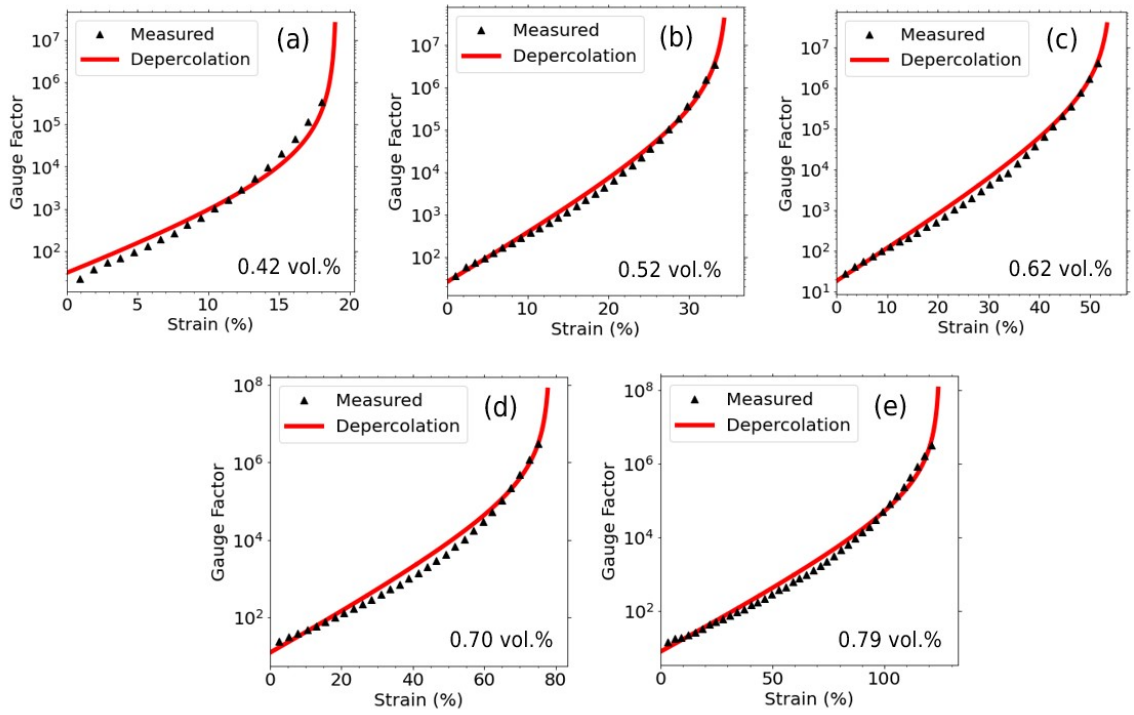

Fig. S11. Gauge factor of SR/rGO strain sensors with respective filler contents of (a) 0.42vol.% (b) 0.52vol.% (c) 0.62vol.% (d) 0.70vol.% (e) 0.79vol.% measured at different strains using the gradient of the calibration curve (resistance change vs. strain). The red lines show the gauge factor predicted by the depercolation model.

Table S1. Results of fitting SR/rGO strain sensing data to the depercolation model.

rGO			G_d	ε_d
vol.%	***wt.%***	***phr***		
0.42	0.74	0.75	25.5 ± 0.9	(19.9 ± 3.5)%
0.52	0.93	0.93	23.7 ± 3.6	(32.9 ± 4.6)%
0.62	1.10	1.11	16.6 ± 2.5	(50.4 ± 10.9)%
0.70	1.23	1.25	10.4 ± 0.7	(79.1 ± 5.8)%
0.79	1.39	1.41	6.9 ± 0.1	(137.3 ± 12.8)%

3 Calibration

3.1 Derivation of the Depercolation Model Equation for Strain

Calibration using the depercolation model requires use of the Lambert W function *W(x)* to calculate the strain,

$$\varepsilon = \varepsilon_d - \frac{1}{G_d} W\left(\frac{R_0 \varepsilon_d G_d e^{\varepsilon_d G_d}}{R}\right) \quad (1)$$

This is because the resistance has a mixed exponential and hyperbolic dependence on strain. Below is the derivation for the equation for strain, starting with the equation for resistance,

$$\frac{R}{R_0} = \frac{e^{G_d \varepsilon}}{1 - \frac{\varepsilon}{\varepsilon_d}} \quad (2)$$

$$\frac{R_0}{R} = \left(1 - \frac{\varepsilon}{\varepsilon_d}\right) e^{-G_d \varepsilon}$$

$$\frac{R_0}{R} = \frac{1}{G_d \varepsilon_d}\left(G_d \varepsilon_d - G_d \varepsilon\right) e^{-G_d \varepsilon}$$

$$\frac{G_d \varepsilon_d e^{G_d \varepsilon_d} R_0}{R} = \left(G_d \varepsilon_d - G_d \varepsilon\right) e^{G_d \varepsilon_d - G_d \varepsilon}$$

Substituting $y = G_d \varepsilon - G_d \varepsilon_d$ gives,

$$G_d \varepsilon_d e^{G_d \varepsilon_d} \frac{R_0}{R} = y e^{y}$$

The Lambert W function is defined by the following equation:

$$y e^{y} = x \;\Leftrightarrow\; y = W(x) \quad [-\frac{1}{e}, \infty)$$

$$y e^{y} = \frac{G_d \varepsilon_d e^{G_d \varepsilon_d} R_0}{R} \;\Leftrightarrow\; G_d \varepsilon_d - G_d \varepsilon = W\left(\frac{G_d \varepsilon_d e^{G_d \varepsilon_d} R_0}{R}\right)$$

$$\therefore \varepsilon = \varepsilon_d - \frac{1}{G_d} W\left(\frac{G_d \varepsilon_d e^{G_d \varepsilon_d} R_0}{R}\right) \quad (1)$$

4 Interparticle Distance Model

4.1 Tunneling Sensitivity

Equating the equation for resistance from the depercolation model with the approximation for nanocomposite resistance according to Simmons' tunneling theory [3] gives the following,

$$\frac{e^{G_d\varepsilon}}{1-\frac{\varepsilon}{\varepsilon_d}} = \frac{N_0}{N}(\varepsilon+1)e^{\gamma s_0\varepsilon},\ \gamma = \frac{4\pi}{h}\sqrt{2m_e\lambda} \tag{3}$$

Solving for the tunneling sensitivity, G_d, gives,

$$G_d = \gamma s_0 + k_N \tag{4}$$

Where k_N is defined by the following equation for the number of conducting pathways, N,

$$\frac{N}{N_0} = (\varepsilon+1)\left(1-\frac{\varepsilon}{\varepsilon_d}\right)e^{-k_N\varepsilon} \tag{5}$$

Rearranging Eq. (5) gives,

$$k_N\varepsilon = \ln(\varepsilon+1) + \ln\left(1-\frac{\varepsilon}{\varepsilon_d}\right) + \ln(N_0) - \ln(N) \tag{6}$$

Tunneling sensitivity is strain-invariant by definition, so assuming that the height of the potential barrier, λ, does not change with increasing strain, we can see from Eq. (4) that k_N is strain-invariant as well. Thus, taking the first derivative of Eq. (6) gives,

$$k_N = \frac{1}{\varepsilon+1} + \frac{1}{\varepsilon-\varepsilon_d} - \frac{1}{N}\frac{dN}{d\varepsilon} \tag{7}$$

We can simplify by considering the point where strain is zero,

$$k_N = 1 - \frac{1}{\varepsilon_d} - \frac{1}{N_0}\frac{dN}{d\varepsilon}\bigg|_{\varepsilon=0}$$

For robust conductive networks the last term should be negligible since the at the lowest strains, the number of conducting pathways is large, and the initial rate of change in number of conductive pathways is small. Therefore, for most nanocomposites, we can approximate that,

$$G_d = \gamma s_0 - \frac{1}{\varepsilon_d} + 1 \quad (8)$$

4.2 Filler Dimensions

Li and Kim [4] used an interparticle distance (IPD) model, in which the filler network consists of homogenously distributed round platelets, to predict the percolation threshold of conducting polymer composites containing disc-shaped nanoparticles with high aspect ratios. They derived that for 3D randomly orientated platelets of diameter, D, and thickness, t, the average separation between platelets is given by,

$$s_0 = \sqrt[3]{\frac{27\pi D^2 t}{4\theta}} - D \quad (9)$$

For a fixed thickness, s_0 is expected to decrease with increasing D (using approximate values of t = 3nm, $\theta = 0.005$). For fixed D we observe that s_0 increases monotonically with t. Substituting in aspect ratio, $\alpha = D/t$, gives,

$$s_0 = D\left(\sqrt[3]{\frac{27\pi}{4\theta\alpha}} - 1\right) \quad (10)$$

For fixed D we observe that s_0 decreases monotonically with α.

Table S2. Predicted effects of filler dimensions on percolation threshold and interparticle distance from Li & Kim 2007 [4].

Increase in platelet property	Percolation threshold [4]	Interparticle distance
Diameter	Decreases	Decreases (in given range)
Thickness	Increases	Increases
Aspect ratio	Decreases	Decreases

4.3 Filler Alignment

For 2D randomly oriented platelets where all platelets are oriented along the axis of conduction, the average separation between platelets is given by [4],

$$s_0 = \sqrt[3]{\frac{2\pi D^2 t}{\theta}} - D \qquad (11)$$

By comparison with Eq. (10), we can predict that the average interparticle distance is higher for a composite consisting of 3D randomly oriented platelets than if the same composite had highly aligned fillers.

References

1. Stylianakis, M.M., et al., *Updating the Role of Reduced Graphene Oxide Ink on Field Emission Devices in Synergy with Charge Transfer Materials.* Nanomaterials, 2019. **9**(2).
2. Compton, O.C. and S.T. Nguyen, *Graphene Oxide, Highly Reduced Graphene Oxide, and Graphene: Versatile Building Blocks for Carbon-Based Materials.* Small, 2010. **6**(6): p. 711-723.
3. Simmons, J.G., *Generalized formula for the electric tunnel effect between similar electrodes separated by a thin insulating film.* Journal of applied physics, 1963. **34**(6): p. 1793-1803.
4. Li, J. and J.-K. Kim, *Percolation threshold of conducting polymer composites containing 3D randomly distributed graphite nanoplatelets.* Composites Science and Technology, 2007. **67**(10): p. 2114-2120.